

Comment

Comment on “Pre-Collapse Space Geodetic Observations of Critical Infrastructure: The Morandi Bridge, Genoa, Italy” by Milillo et al. (2019)

Riccardo Lanari ^{1,*}, Diego Reale ¹, Manuela Bonano ^{1,2}, Simona Verde ¹,
Yasir Muhammad ^{1,3}, Gianfranco Fornaro ¹, Francesco Casu ¹ and Michele Manunta ¹

¹ Institute for the Electromagnetic Sensing of the Environment—National Research Council (IREA-CNR), Via Diocleziano 328, 80124 Naples, Italy; reale.d@irea.cnr.it (D.R.); bonano.m@irea.cnr.it (M.B.); verde.s@irea.cnr.it (S.V.); yasir.m@irea.cnr.it (Y.M.); fornaro.g@irea.cnr.it (G.F.); casu.f@irea.cnr.it (F.C.); manunta.m@irea.cnr.it (M.M.)

² Institute of Methodologies for Environmental Analysis—National Research Council (IMAA-CNR), C. da S. Loja-Z.I., 85050 Tito Scalo, Italy

³ Department of Engineering, University of Naples “Parthenope”, Centro Direzionale Isola C4, 80133 Naples, Italy

* Correspondence: lanari.r@irea.cnr.it

Received: 9 July 2020; Accepted: 1 December 2020; Published: 8 December 2020



Abstract: We present in this comment a Multi-Temporal SAR Interferometry (MT-InSAR) analysis showing that the results published by Milillo et al. (2019) in the Remote Sensing Journal, presenting the evidence of space geodetic observations relevant to displacements occurring before the collapse of the Morandi Bridge, happened in Genova (Italy) on the 14 August 2018, are questionable. In particular, we focus on the InSAR results obtained by Milillo et al. (2019) by processing the 3 m × 3 m resolution COSMO-SkyMed (CSK) data collected from ascending and descending orbits on the area of interest. These results, thanks to the high spatial resolution and the short revisit time characterizing this multi-orbit SAR dataset, represent the cornerstone of their analysis. The main findings of their study allow Milillo et al. to conclude that the InSAR processing of this COSMO-SkyMed dataset reveals the increased deformation magnitude over time of points located near the strands of the deck next to the collapsed pier, between 12 March 2017 and August 2018. In this comment, we show the results obtained by the IREA-CNR SAR team after processing the same ascending and descending CSK dataset, but by using two alternative and independent processing techniques: the Small Baseline Subset (SBAS) and the Advanced Tomographic SAR (TomoSAR) approaches, respectively. Our analysis shows that, although both the SBAS and the TomoSAR analyses allow achieving denser coherent pixel maps relevant to the Morandi bridge, nothing of the pre-collapse large displacements reported in Milillo et al. (2019) appears in our results, leading us to deeply disagree with the findings of their InSAR analysis.

Keywords: bridge collapse; infrastructures monitoring; InSAR; deformation time series; SBAS; TomoSAR

1. Introduction

On the 14 August 2018, the Polcevera viaduct—known as the Morandi bridge—in the city of Genova (Italy), which connects the eastern and western sides of the Genova metropolitan area and represents the main highway to link Southern France and Northern Italy, suffered the collapse of a section of the deck approximately 240 m long, adjacent to pier 9, close to the Polcevera river, causing the death of 43 people, and leaving 11 injured [1].

Following the bridge collapse, the Italian Civil Protection Department together with the Italian Space Agency (ASI) asked some Italian research groups highly qualified in Synthetic Aperture Radar Interferometry (InSAR) techniques to perform advanced InSAR analyses, based on the use of SAR data collected by the European C-band Sentinel-1 and the Italian X-band COSMO-SkyMed (CSK) constellations and relevant to the pre-event time interval, in order to capture any possible early displacements associated with structural failures. Although performed in a very short time frame, immediately after the bridge failure, such analyses did not reveal significant displacements in correspondence to the collapsed pier.

More recently, in 2019 Milillo et al. [2] carried out an InSAR analysis based on the processing of SAR data collected by the ENVISAT, Sentinel-1 and CSK sensors. In particular, their processing of the $3\text{ m} \times 3\text{ m}$ resolution CSK data collected from ascending and descending orbits represents the cornerstone of their analysis thanks to the high spatial resolution and the short revisit time characterizing this multi-orbit SAR dataset. The results presented in [2] allow the Authors to conclude that the CSK-based InSAR analysis reveals an increased deformation magnitude over time in correspondence to points located near the strands of the deck next to the collapsed pier, between 12 March 2017 and the beginning of August 2018. These findings clearly disagree with those of the above-mentioned expeditious analyses carried out immediately after the bridge collapse.

Accordingly, in this study, we focus on the same ascending and descending CSK datasets investigated in [2]. Note that they both have a rather long temporal extension (from January 2011 to August 2018), thus guaranteeing a very reliable quality of the InSAR products (deformation time series and mean velocity maps). Moreover, the characteristics of the CSK SAR system, in particular, the resolution and the transmitted radiation wavelength, have a large impact on the results retrieved through the InSAR analysis, in terms of measurement density and mapping capabilities, as well as sensitivity and accuracy. Indeed, the shorter wavelength of the X-Band CSK sensors (about 3.1 cm wavelength) provides higher sensitivity to slighter surface displacements, like those related to thermal dilation effects. Additionally, the fine spatial resolution ($3\text{ m} \times 3\text{ m}$) characterizing the Stripmap mode of the exploited CSK data leads to an improved density of measurement points (i.e., coherent pixels) over built-up structures, thus allowing to carry out detailed deformation analyses relevant to complex infrastructures like the Morandi bridge [3,4]. Moreover, thanks to the rather large orbital baseline tube of the CSK constellation, the investigated coherent SAR pixels may be geolocalized with a significant accuracy (on the order of a few meters). Finally, the availability of SAR data collected from both ascending and descending orbits permits us to verify the consistency of the InSAR results obtained from very different illumination geometries. In particular, in the presented study, we reprocessed the overall ascending and descending CSK dataset analyzed in [2] by exploiting two independent SAR processing techniques: the Small Baseline Subset (SBAS) [5–7] and the Advanced Tomographic SAR (TomoSAR) [8,9] approaches, respectively. These two methods are nowadays well-established tools for the investigation of the temporal evolution of displacements affecting buildings and infrastructures [10–20].

Our findings, resulting from the independent processing of each dataset, lead us to conclude that we do not find any evidence of the pre-collapse displacements reported in [2] in pixels located near the strands of the deck next to the collapsed pier.

2. Exploited Data and Multi-Temporal SAR Techniques

In this section, we summarize the main characteristics of the exploited CSK dataset and briefly present the main rationale of the two methods we applied in order to retrieve the deformation time series which are the key objectives of the presented analysis.

2.1. CSK Dataset

The MT-InSAR analysis presented in this work involved the processing of two different datasets acquired by the CSK constellation, both on ascending and descending orbits of the satellites (see Figure 1

for the representation of the ground coverage of the two CSK frames), over the time interval extending from January 2011 to August 2018 (immediately before the Morandi bridge collapse) on an area close to the Morandi bridge, in the city of Genova (North Italy). More specifically, the two datasets are composed of 132 and 134 images for the ascending and descending passes, respectively. For both datasets, the acquisition mode is the H-IMAGE, corresponding to the standard Stripmap acquisition mode [21], characterized by a ground spatial resolution of about $3\text{ m} \times 3\text{ m}$ in azimuth (along-track) and slant-range (cross-track) directions [22]. The reference acquisition beam is the H4-05 for the ascending dataset and H4-01 for the descending one, corresponding to an incidence angle at scene center of about 34° and 27° , respectively. The key parameters for the two SAR datasets exploited in this work are briefly summarized in Table 1.



Figure 1. Representation of the two exploited COSMO-SkyMed (CSK) frames acquired from ascending (black rectangle) and descending (red rectangle) orbits, superimposed on a Google Earth optical image. Note that the white rectangle falling within the two frames represents the area of interest surrounding the Polcevera viaduct close to the Morandi bridge.

Table 1. Main characteristics of the exploited CSK datasets.

	Ascending	Descending
Wavelength		~3,1 cm
Acquisition mode		H-IMAGE
Average look angle	~ 34°	~ 27°
Spatial resolution of the interferometric data		~ $3\text{ m} \times 3\text{ m}$
Beam-ID	H4-05	H4-01
Time interval	23 February 2011–5 August 2018	7 January 2011–6 August 2018
Number of acquisitions	132	134

The distributions of the selected interferometric SAR acquisitions in the temporal/perpendicular baseline plane for the two CSK datasets are pictorially shown in Figure 2. It is worth remarking the temporal correlation of the perpendicular baseline distribution (and thus of the corresponding orbits), which has to be properly taken into account throughout the interferometric processing.

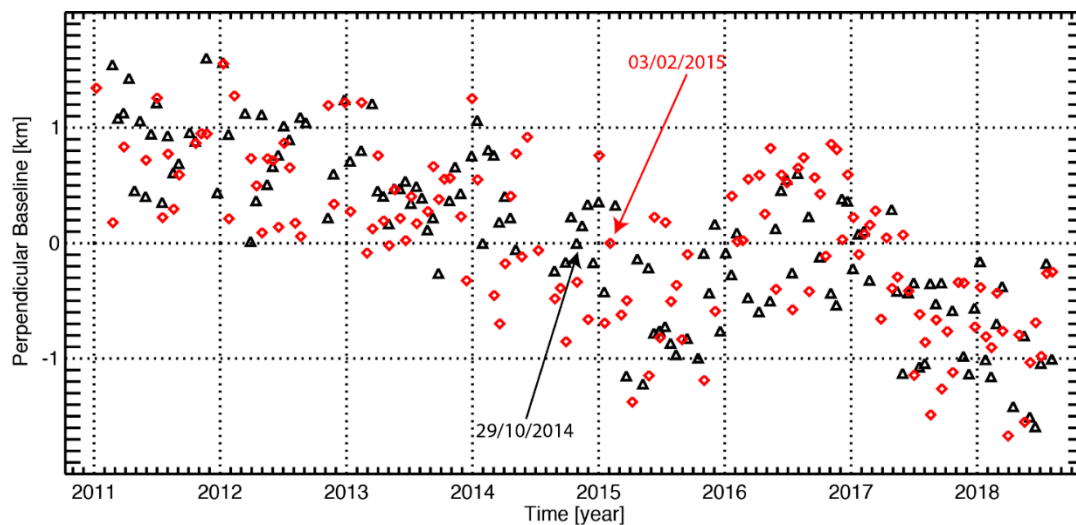


Figure 2. SAR data representation in the temporal/perpendicular baseline plane for the two CSK datasets relevant to the area of interest. The black triangles and the red diamonds represent the ascending and descending acquisitions, respectively. The reference (master) images selected for the processing of the ascending and descending CSK datasets, relevant to the 29 October 2014 and to the 3 February 2015 acquisitions, respectively, are identified by the arrows.

In this paper, we focus on the analysis of the pre-collapse displacements associated with the Morandi bridge (see the white rectangle in Figure 1 for its location), which are extensively investigated through two independent MT-InSAR techniques referred to as the Small Baseline Subset (SBAS) and the Advanced Tomographic SAR (TomoSAR) approaches. A brief summary of these two techniques is reported in the following two paragraphs.

2.2. The SBAS Technique

The available ascending and descending CSK datasets were processed through the SBAS technique [5–7], which is an advanced SAR Interferometry method that allows retrieving useful information on the spatial and temporal patterns of the detected radar Line of Sight (LOS)-projected displacements, through the generation of deformation time series and mean velocity maps. The SBAS approach relies on a proper selection of the SAR data pairs used to generate a multi-temporal sequence of differential interferograms (i.e., the phase difference between two SAR images collected over the same area at different epochs), which are characterized by a small separation between the acquisition orbits (short temporal and perpendicular baselines).

The use of small spatial and temporal baselines of the generated interferograms permits mitigating the noise effects (decorrelation phenomena) that affect the interferometric pairs [23], thus increasing the spatial density of the retrieved InSAR measurements (number of coherent pixels), especially in semi-urbanized and rural areas. The deformation time series (and the corresponding mean velocity maps) are then computed by solving a linear system of equations in a least-squares sense, with a minimum norm energy constraint (the Singular Value Decomposition—SVD technique is applied in presence of independent acquisition subsets separated by large baselines), and with an accuracy of about 1–2 mm/year for what concerns the mean deformation velocity information and 5–10 mm for the single deformation measurement [3,24]. Moreover, within the SBAS processing chain, a filtering operation is performed to detect and remove atmospheric artifacts from the displacement time series [5].

One key point of the SBAS algorithm is the capability of performing both multi-sensor [7,25] and multi-scale [6,10] deformation analysis; in particular, the latter allows generating InSAR products at two spatial resolution scales, referred to as a regional and a local one. This is accomplished by dealing with multi-look interferograms (regional scale analysis with a typical spatial resolution of about 30–90 m), and full-resolution interferograms (local scale analysis, generated from the single-look data,

with the full spatial resolution, 3 m for this CSK case), respectively. The regional scale is suitable to detect low-pass signal components, such as deformation related to large areas or atmospheric artifacts, whereas the local scale one is particularly appropriate to investigate high-pass signals, such as those related to very small displacements associated with infrastructures or parts of them. Such a pioneer peculiarity of the two-scale SBAS approach has influenced the development of various MT-InSAR techniques and has deeply contributed to its wide dissemination within the Solid Earth science community, since it reveals to be particularly suitable for a wide range of applications, from civil protection scenarios (natural hazard risk prevention and mitigation, volcano, seismic events, landslides) to anthropogenic contexts (extended urban areas, archaeological and historical sites, oil–gas extraction, structures and transport infrastructures, mine activity, etc.) [13,14,26–34].

In this work, the two-scale SBAS approach [6] was exploited to process both the ascending and descending CSK datasets of our case study, allowing us to deeply investigate the spatial and temporal evolution of the possible pre-event displacements affecting the Morandi bridge. Moreover, additional information on the residual topography (with respect to the used DEM) of the coherent pixels, as well as on the thermal dilation components associated with the daily temperatures, is also retrieved.

2.3. The TomoSAR Technique

SAR Tomography (TomoSAR) [9] is a processing technology that extends the Persistent Scatterers Interferometry (PSI) [35,36] method for the analysis of pixels at the full available resolution of the data. It brings the imaging concept of the synthetic aperture in the along-track direction, which allows achieving azimuth high-resolution SAR images, also in a third dimension, referred to as elevation, associated with the spatial (perpendicular) separation of the orbits and orthogonal to the azimuth/slant-range plane. SAR Tomography switches the processing from the matching of the measured phases with the expected model related to the parameters of interest, i.e., height and velocity, firstly introduced by PSI phase matching into the imaging of the backscattered profile [8,9]. SAR Tomography extends the synthetic aperture processing, which allows achieving high spatial resolution images, to the height direction based on the availability of multiple observations from slightly different orbits. Therefore, the signal backscattered from ground objects can be focused at high resolution also in the third dimension (height), hence, the name *3D imaging* [37–39]. By including in the processing also the temporal diversity of the acquisitions, space/velocity model (*4D imaging*) is derived by extending the 3D imaging concept into the time domain to measure the deformation parameters of any temporal coherent Persistent Scatterer (PS) in the focused 3D space [8,40]. The imaging domain can be further extended to even monitor the slight movements induced by the thermal dilation of the imaged structures [19,41,42].

In this paper, TomoSAR processing is performed according to the procedure described in [9]. It is based on a cascade of two main blocks operating at different spatial scales: the first block, operating on a set of spatially averaged interferograms belonging to a grid set according to the Small-Baseline criteria [5,43], allows carrying out the estimation and compensation of the atmospheric phase patterns, as well as an estimation of the non-linear deformation at a lower resolution. These two-phase component estimates provide the necessary input for the phase calibration of the data which is mandatory for the implementation of the TomoSAR imaging at the full resolution. This latter, which represents the second and core step of the processing, is implemented through the procedure in [8] based on the exploitation of the Beamforming filter, i.e., the matched filter, which measures the correlation of the measured phase vector with the expected phase model accounting for the geophysical parameters of interest.

For this specific analysis, the TomoSAR processing was carried out through the implementation of 5D imaging, accounting for residual topography, linear temporal deformation and possible deformation components correlated with the daily average temperature of the area induced by thermal dilation of materials [41]. The analysis was limited to the single scatterers: the detection of output measurements points was implemented by applying the Generalized Likelihood Ratio Test (GLRT) decision scheme [44] which is based on the comparison of the normalized correlation among the measurement vector and

the expected phase model, with a threshold set according to the designed probability of false alarm. The test is applied to every image pixel: neither pre-processing candidates selection nor post-processing outlier filtering is performed.

3. Results

The results of the CSK analysis at the full available spatial resolution obtained through the independent implementation of the SBAS and of the TomoSAR processing techniques in the area of interest, including the Morandi bridge, are reported in Figure 3.

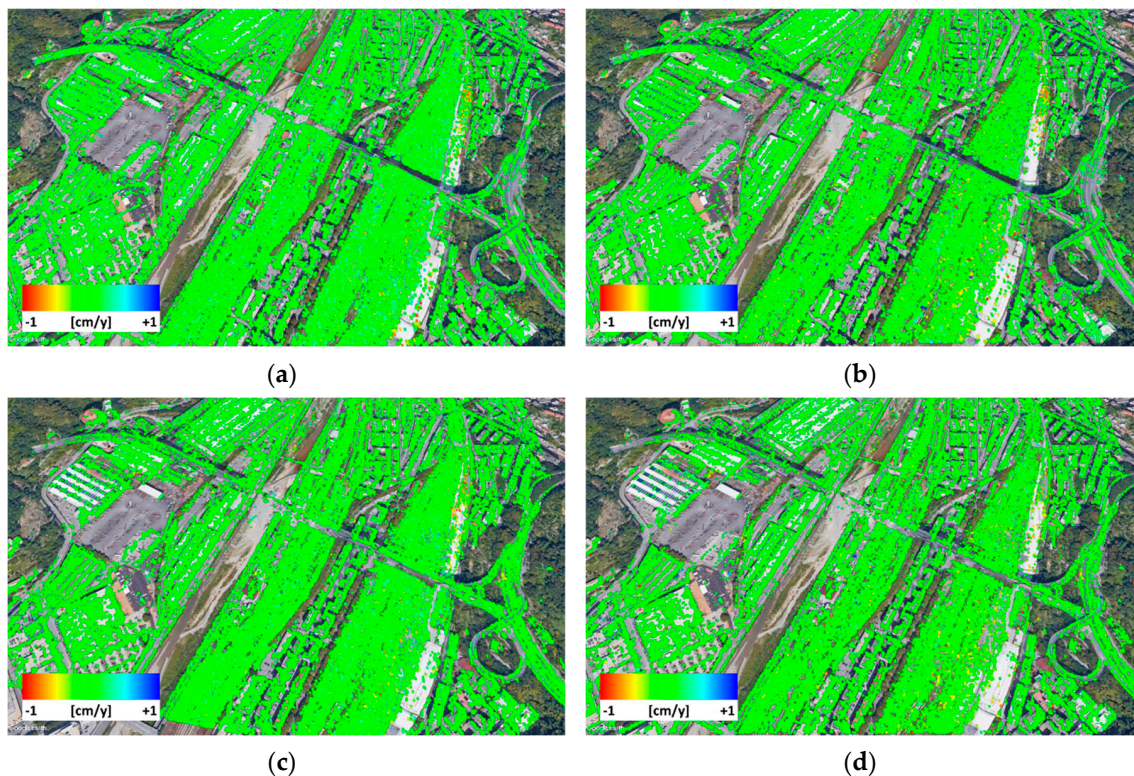


Figure 3. Mean deformation velocity maps over the area of interest for (a) Small Baseline Subset (SBAS) and (b) TomoSAR processing results achieved for the ascending dataset, and (c) SBAS and (d) TomoSAR results relevant to the descending dataset. Colormap is set according to the estimated velocity with the convention that negative values correspond to departure from the sensor along the LOS. Reference pixels for SBAS and TomoSAR processing are located at $[44.4130^\circ, 8.8879^\circ]$ and $[44.4160^\circ, 8.8738^\circ]$, respectively, which are in stable areas far away from the bridge.

This figure shows the estimated LOS deformation mean velocity maps for the ascending (upper row) and descending (bottom row) datasets relevant to both the SBAS (left column) and TomoSAR (right column) processing techniques. The maps are represented in the North-oriented geometry; for all the results, the colormap is set according to the estimated mean velocity with the typical convention that negative velocities are associated with scatterers that are moving away from the sensor along the LOS. The images show a very high density of measurement points, with a good agreement between the results obtained through the two MT-InSAR processing techniques, both in terms of coverage and density, and measured deformation. A comparable density of measurement points is finally achieved on both ascending and descending datasets, thus proving a satisfactory sampling of the data over the two orbits. Note also that the reference pixels for the two MT-InSAR processing are independently selected in different stable areas far away from the bridge: the agreement of the achieved results demonstrates the robustness of the applied processing approaches with respect to the spatial reference selection. The position of the Morandi bridge is easily recognizable: being a raised structure, it causes

the presence of a sort of straight strip, induced by the shadow effect, crossing the image from left to right, characterized by the absence of measurement points. Bridge points are located on the southern and northern boundaries of that strip for ascending and descending data, respectively. By analyzing the maps, no significant deformation is, at that scale, identified.

The detailed analysis of the results over the Morandi bridge is now in order. To assess the bridge deformation behavior in the observed period, we firstly isolated, from the overall results in Figure 3, the measurement points located at the bridge deck. Specifically, we firstly isolated measurement points located on the northern roadway, approximately framed within the yellow rectangle in Figure 4. A threshold of 40 m on the estimated height, above the sea level, of the coherent pixels was also applied to isolate the raised points, only. The distribution of the detected pixels shows a concentration near the support towers. The lack of coherent points in the central part of the suspended deck may be induced by large non-linear displacements possibly induced by vibration effects and wind.

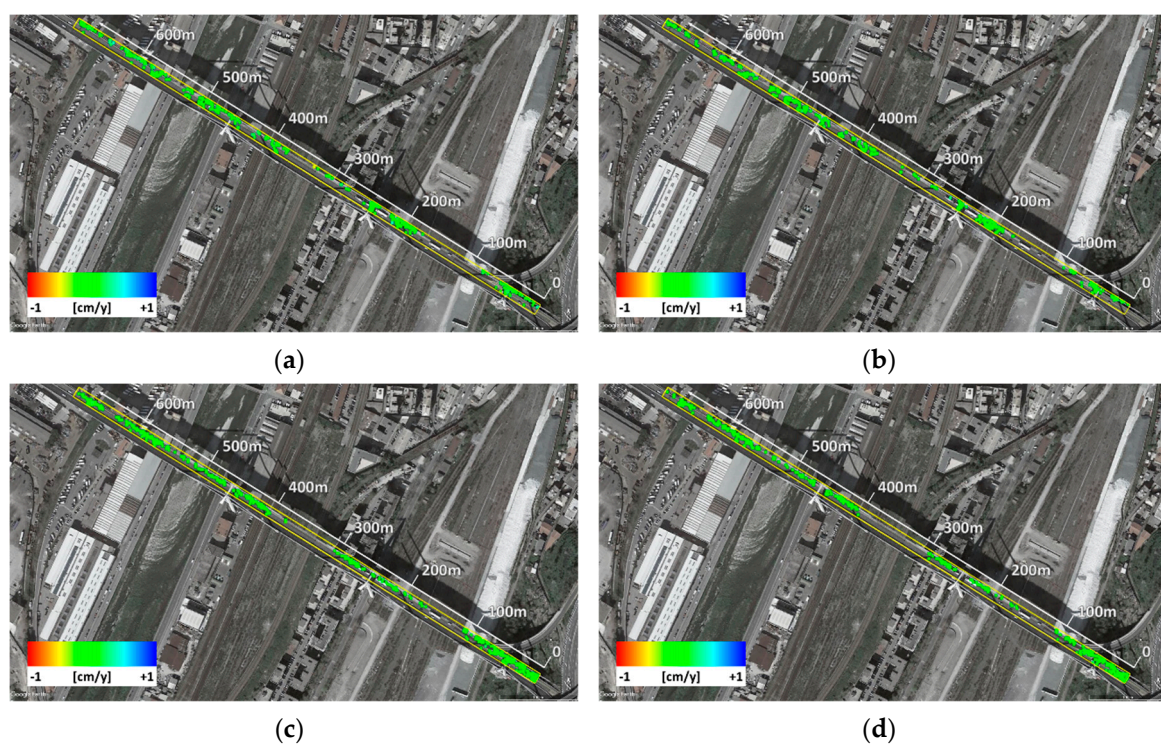


Figure 4. Highlight on the coherent pixels located within the yellow frame, corresponding to the northern roadway, for (a) SBAS and (b) TomoSAR processing results achieved for the ascending dataset, and (c) SBAS and (d) TomoSAR results relevant to the descending dataset. Colormap is set according to the estimated velocity with the convention that negative values correspond to departure from the sensor along the Line of Sight (LOS). The white graduated axis represents the longitudinal coordinate of the yellow rectangle whose origin is set at the southern/eastern end of the bridge.

The estimated height of the selected pixels, represented by red diamonds, is provided in the plots depicted in Figure 5. The horizontal axis represents the longitudinal coordinate of the yellow rectangle, i.e., the length from its origin, conventionally set at its eastern end and approximately corresponding to the initial part of the bridge, as also pointed out by the graduated scale in Figure 4. The straight distribution of pixels at almost constant height on the bridge deck is easily recognizable; moreover, the triangular shape, particularly evident in the descending dataset results, also allows recognizing the first tower from East. Remarkably, the very high-resolution capability of the CSK sensors allows monitoring even pixels located along the tie rods cables. In the same figure, the black diamonds represent the coherent pixels that do not exceed the height threshold which likely belong to ground structures: the rectangular shape determined by the pillars of the second tower is recognizable at about

250–300 m from the origin of the line. By comparing the results of the first and second row, the different coverage induced by the sensor LOS visibility over the two opposite orbits is evident. On the contrary, no significant differences are met by the comparison of the coherent pixel distributions, for the same dataset, achieved by the two processing techniques. Finally, the plot of the estimated deformation mean velocity over the selected points, along the longitudinal coordinate of the yellow rectangle, is provided in Figure 6: it confirms that no significant deformation was detected along the whole northern roadway of the bridge deck. Results are very consistent among the different processing outputs and datasets. Note that the coherent pixel detected in the results of the TomoSAR processing of the descending dataset, i.e., the plot in Figure 6d, at approximately 450 m from the line origin, which exhibits a linear deformation of more than 1.5 cm/year, is very likely related to a false alarm which, however low was the desired probability of false alarm, passed the GLRT detection stage. It is worth remembering that, as already mentioned, no further post-processing outlier filtering is performed.

The point is surrounded by a large density of coherent pixels concentrated in a few meters which exhibit no significant deformation. It is very unlikely that, given this spatial distribution of close PSs, a ground pixel could exhibit such a significantly different deformation behavior from its neighboring PS. Moreover, this anomalous behavior is detected neither in the SBAS results on the same dataset, nor in both SBAS and TomoSAR results related to the ascending dataset.

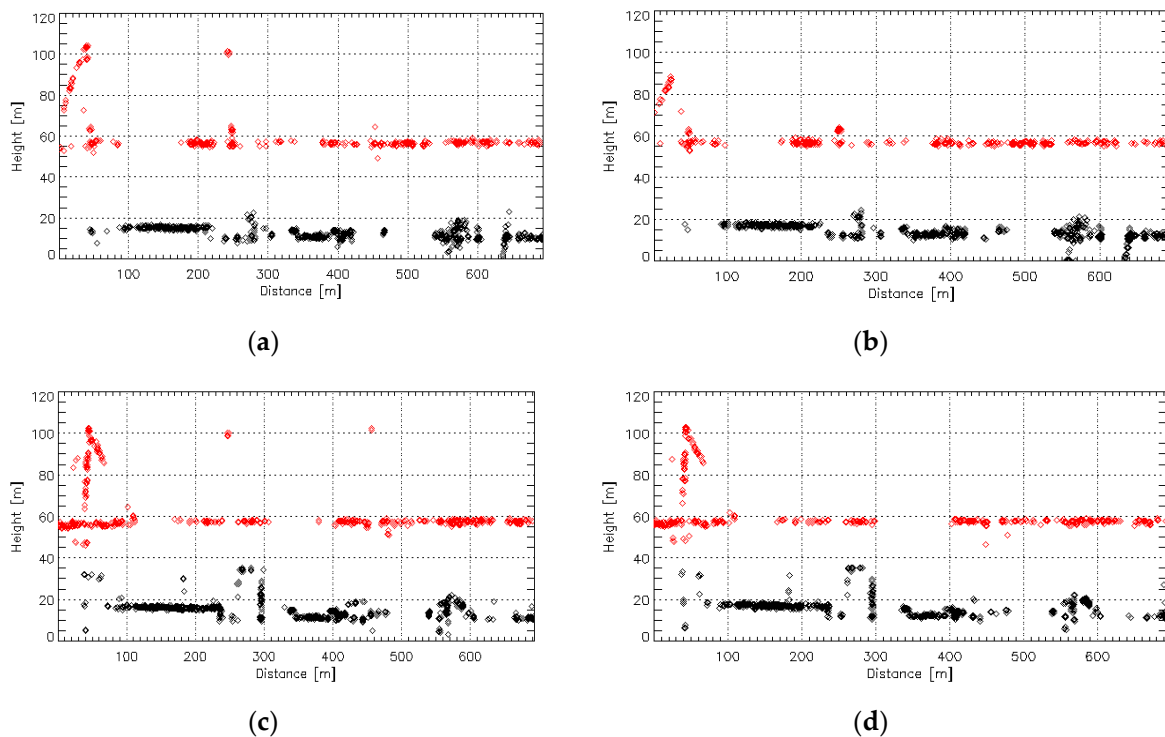


Figure 5. Plots of the estimated height of the coherent pixels located within the yellow rectangle in Figure 4 for (a) SBAS and (b) TomoSAR results achieved for the ascending dataset, and (c) SBAS and (d) TomoSAR results relevant to the descending dataset. Red and black diamonds correspond to measurement points located on the roadway, pillars and cables and at the ground level, respectively. Horizontal axis corresponds to the longitudinal distance from the origin of the yellow rectangle located at its southern/eastern end, as reported by the white graduated scale in Figure 4.

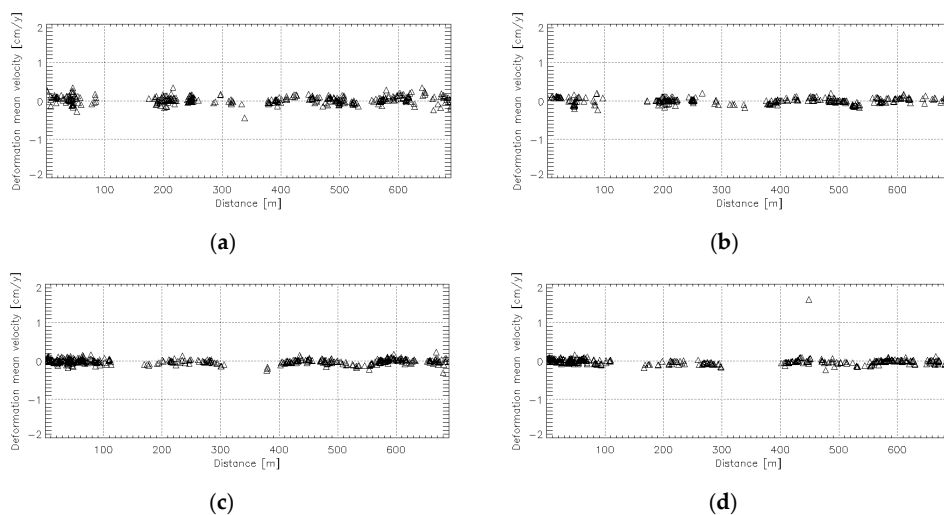


Figure 6. Plots of the estimated deformation mean velocity of the coherent pixels located at the northern roadway level within the yellow rectangle in Figure 4 for the (a) SBAS and (b) TomoSAR processing results achieved for the ascending dataset, and (c) SBAS and (d) TomoSAR results relevant to the descending dataset. Horizontal axis corresponds to the longitudinal distance from the origin of the yellow rectangle located at its southern/eastern end, as reported by the white graduated scale in Figure 4.

A close-up analysis of the collapsed pillar is now in order: Figure 7 shows a zoom in the area of interest of the collapsed pillar of the measurement points of Figure 4, i.e., located on the northern roadway of the bridge for (a) SBAS and (b) TomoSAR processing techniques over the ascending dataset, (c) SBAS and (d) TomoSAR processing ones over the descending dataset. For these selected points, the time series of the estimated deformation are shown in Figure 8. Apart from a typical seasonal trend limited to a 3 cm range, all measurement points do not undergo any significant deformation. Again, a very high correlation of estimated time series is found. In Figure 8d the single anomalous deformation trend is related to the false alarm point whose anomaly was previously discussed. The time series associated with other neighboring points do not show any significant behavior: this further confirms the hypothesis of the false alarm detection.

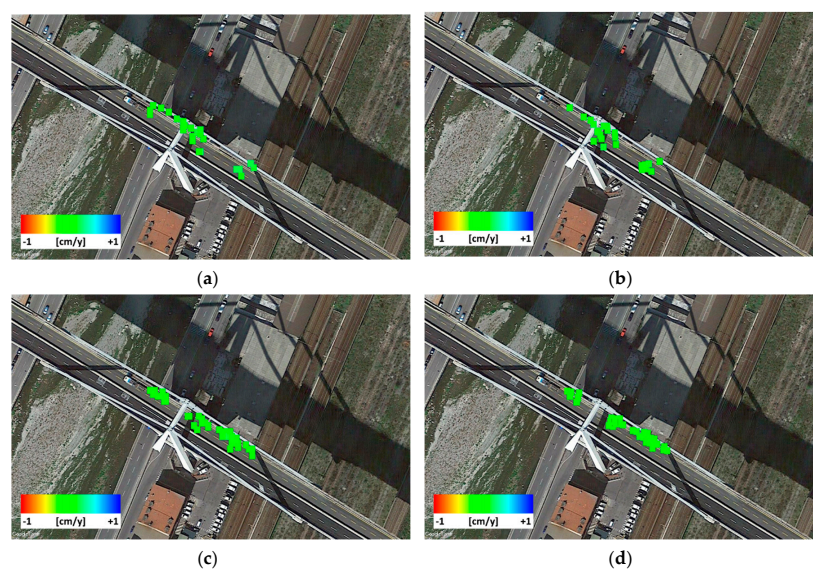


Figure 7. Zoom of Figure 4 in the area of interest related to the collapsed pillar, (a) SBAS and (b) TomoSAR processing results over the ascending dataset, and (c) SBAS and (d) TomoSAR results relevant to the descending dataset.

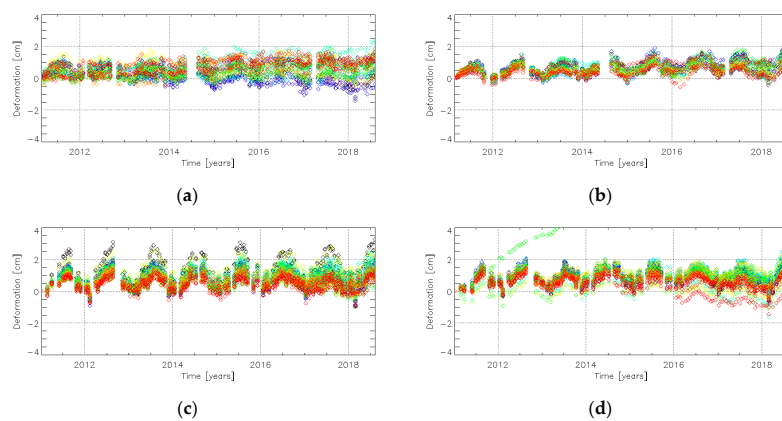


Figure 8. Plots of the estimated deformation time series for the coherent pixels in the area of interest related to the collapsed pillar provided in Figure 7 for (a) SBAS and (b) TomoSAR results relevant to the ascending dataset, and (c) SBAS and (d) TomoSAR results for the descending dataset.

A similar analysis was performed on the southern roadway of the bridge deck. Similar to the northern roadway case, the coherent pixels located at the bridge deck on the southern roadway were isolated. The results are provided in Figure 9, in which the analysis was limited to the points located within the red rectangle and characterized by an estimated height greater than 40 m above the sea level. The plots of the estimated height for the selected pixels, represented as red diamond, and for the ground ones (black diamonds) are reported in Figure 10. Again, the very high CSK resolution allows easily recognizing the first tower and, particularly on the descending dataset, the stay from the top of the tower to the bridge deck, as well as pillars of second and third towers. These plots also highlight the significant different coverage between the ascending and descending datasets on the southern flank of the bridge: because of the significant shadow effect on the descending dataset, the density is drastically reduced on the bridge deck whereas even almost no coherent pixel is detected on the ground segment underlying the southern roadway of the bridge. As for the northern roadway, the plots of the estimated deformation mean velocity within the red rectangle, provided in Figure 11, do not show any significant deformation of interest neither on the pillars, nor at the deck level and specifically in correspondence with the connections of the stay-cables. It is worth noting that, despite the choice of the reference pixels far away from the area of interest, the coverage over the bridge is fairly dense.

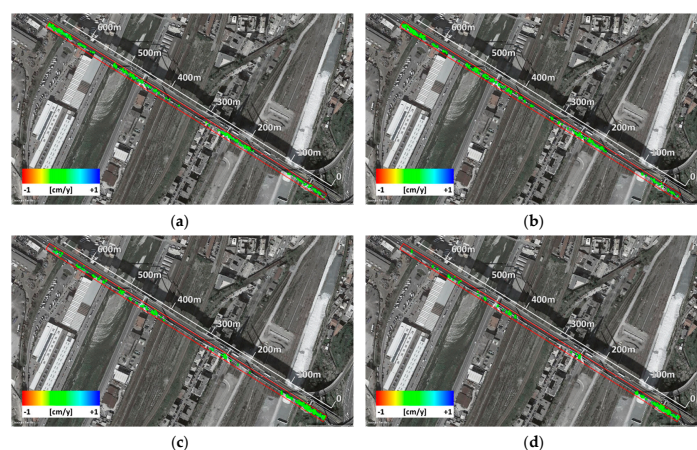


Figure 9. Highlight on the measurement points located within the red frame, corresponding to the southern roadway for (a) SBAS and (b) TomoSAR processing results related to the ascending dataset, (c) SBAS and (d) TomoSAR results relevant to the descending dataset. Colormap is set according to the estimated velocity with the convention that negative values correspond to departure from the sensor along the LOS. The white graduated axis represents the longitudinal coordinate of the red rectangle whose origin is set at the southern/eastern end of the bridge.

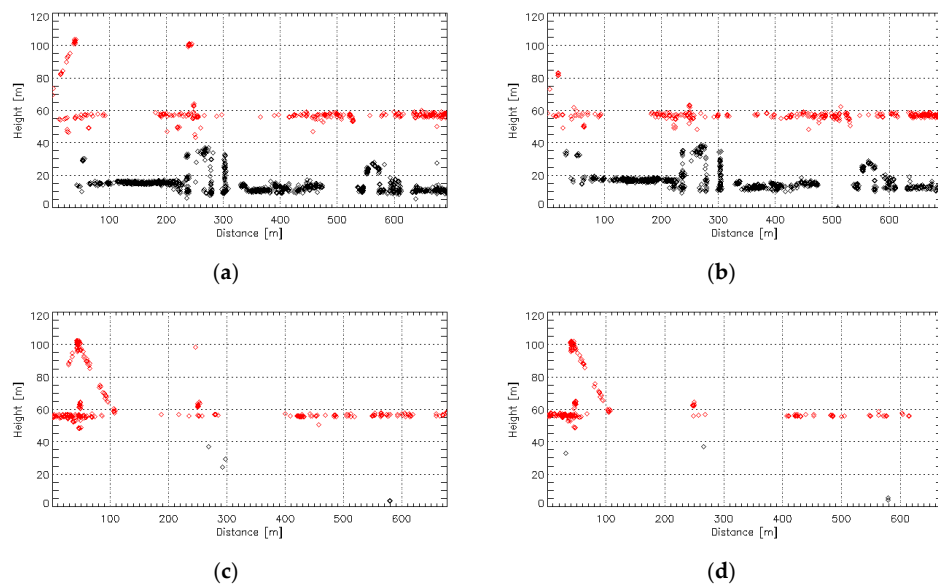


Figure 10. Plots of the estimated height of the coherent pixels located within the red rectangle in Figure 9 for the (a) SBAS and (b) TomoSAR processing results related to the ascending dataset, and (c) SBAS and (d) TomoSAR results relevant to the descending dataset. Red and black squares correspond to measurement points located at the roadway, pillars and cables and at the ground level, respectively. Horizontal axis corresponds to the longitudinal distance from the origin of the red rectangle located at its southern/eastern end, as reported by the white graduated scale in Figure 9.

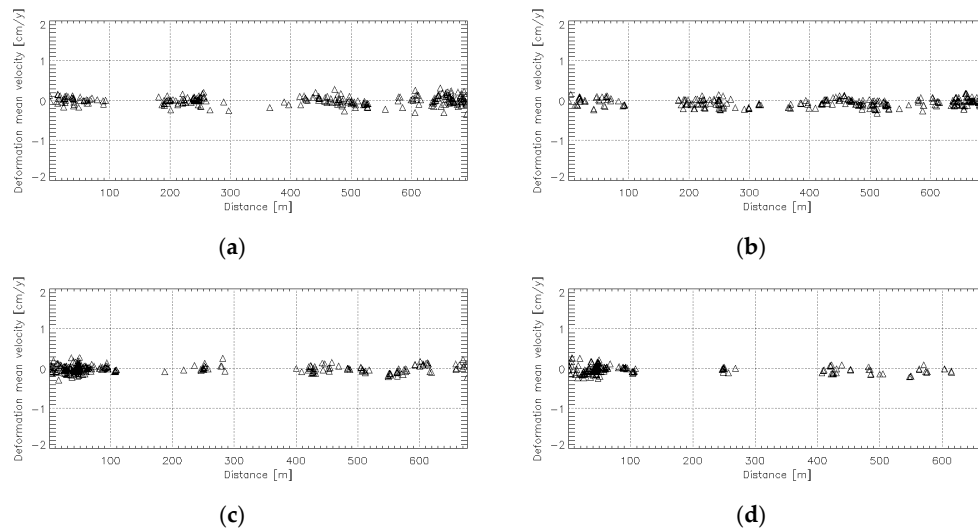


Figure 11. Plots of the estimated mean deformation velocity of the coherent pixels located at the southern roadway level within the red rectangle in Figure 9 for (a) SBAS and (b) TomoSAR processing results of the ascending dataset, and (c) SBAS and (d) TomoSAR results relevant to the descending dataset. The horizontal axis corresponds to the longitudinal distance from the origin of the red rectangle located at its southern/eastern end, as reported by the white graduated scale in Figure 9.

The stable behavior is also confirmed by the close-up analysis in Figure 12, where the pixels located in correspondence to the tower of interest were isolated. For each of these points, the estimated time series depicted in Figure 13 confirm the prevailing seasonal behavior.

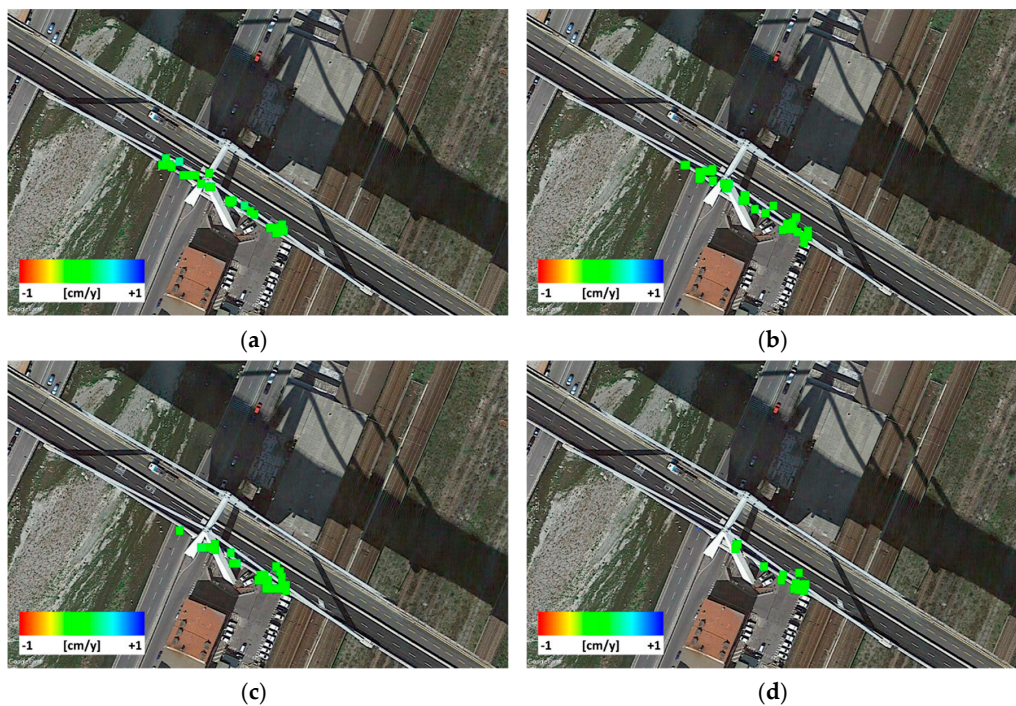


Figure 12. Zoom of Figure 9 in the area of interest related to the collapsed pillar, (a) SBAS and (b) TomoSAR processing results over the ascending dataset, and (c) SBAS and (d) TomoSAR processing results related to the Descending dataset.

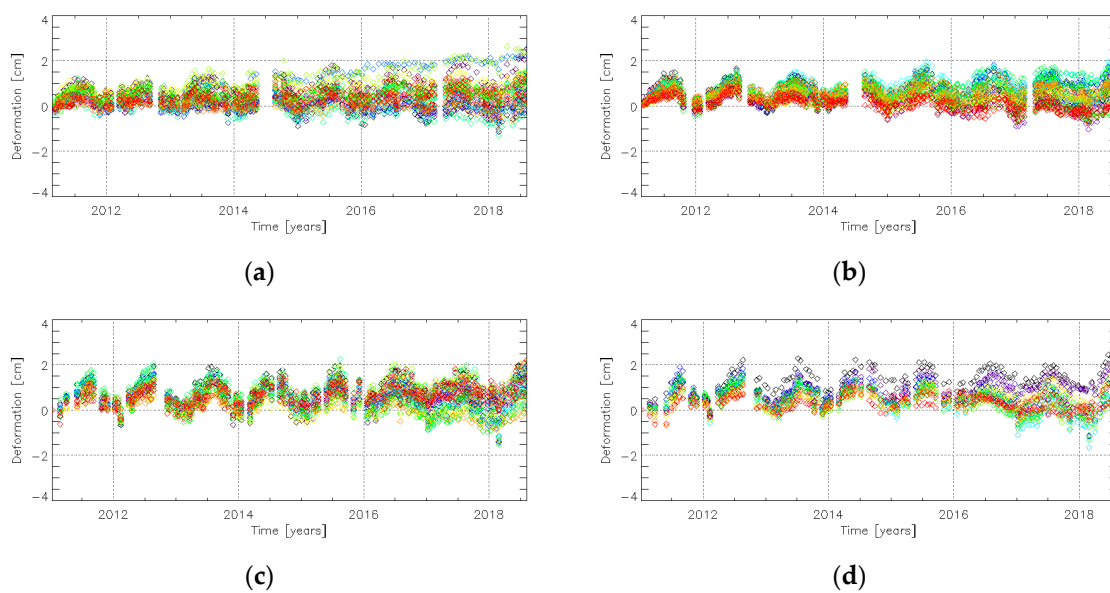


Figure 13. Plots of the estimated deformation time series for the coherent pixels in the area of interest of the collapsed pillar provided in Figure 12 for the (a) SBAS and (b) TomoSAR results achieved for the ascending dataset, and (c) SBAS and (d) TomoSAR results related to the descending dataset.

In order to further provide information about a possible precursor, our displacement study also includes the analysis of the detected PS located at the ground level in correspondence with the collapsed tower. These results, provided in Figures S1 and S2 in the Supplementary Materials, further confirm that no significant displacements were detected.

As a final point, it is once again worth remarking that the results achieved by exploiting the two independent SBAS and TomoSAR approaches are in very good agreement, regardless of the reference pixels selection, thus confirming the robustness of the applied MT-InSAR processing approaches.

In summary, our analysis of the PS detected on the bridge deck shows a great similarity of the results in terms of coverage and measurements and specifically, all the results agree on the fact that, apart from a seasonal trend, no significant deformation trend was observed. This is quite evident by the analysis of the deformation time series and related mean velocities in correspondence to the Morandi bridge obtained by exploiting both ascending and descending data and both the SBAS and the TomoSAR MT-InSAR approaches.

4. Discussion and Conclusions

The monitoring of civil infrastructures as road and railroad bridges is envisaged in order to follow their health conditions and to sort out possible actions for their safety and maintenance over time, thus reducing material and economic losses and, most of all, preserving human lives. Recent estimates demonstrate that the number of bridges in Italy to be assessed after a 50-year service life runs around 50,000 [45]. Currently, the structural health monitoring is mainly based on a visual inspection and accurate in-situ and embedded measurement systems directly installed on the investigated structure, resulting in complex and expensive surveys, which inevitably limit the surveillance to very restricted areas or to single infrastructures. The widespread development of Earth Observation (EO) technologies over the last decades has allowed the detection and monitoring from space of surface displacements related to very large areas and with high accuracy. In this framework, the innovation brought by the MT-InSAR techniques represents very valuable solutions to provide systematic, large scale displacement measurements related to infrastructures, able to simultaneously detect and analyze the deformation of hundreds of road and railroad bridges at relatively low costs. Such measurements, properly integrated with in-situ investigations and damage assessment models derived from structural engineering, may support actions for pre-emptive bridge rehabilitation and decision-making actors [11].

However, to properly move from a scientific context to a fully operative scenario, it is mandatory to deal with consolidated integrated procedures that are able to reduce the false alarm probability within the retrieved InSAR products, by minimizing the possible false positive and negative detections. Indeed, the false alarm issues strongly impact the suitability of InSAR techniques in operative contexts that can support the decision-makers. In particular, the false positives can make negligible the benefits of EO-based techniques in supporting well-focused in-situ surveys and, furthermore, can generate a strong impact on the population when not carefully verified information are disseminated, whereas the false negatives strongly jeopardize the monitoring capability of this technology by leading, in the worst cases, to the lack of identification of possible pre-event signals of future structural failures, with consequent human casualties.

These issues have to be addressed with a twofold approach, involving both the maturity of the exploited InSAR techniques and the related expertise of the end-users. The former concerns the development of accurate and highly verified InSAR techniques, as well as a deep scientific assessment of their maturity in a branched out number of use-cases to demonstrate their usefulness and effectiveness in real operative scenarios. The latter requires knowledge and consolidated experience of the users when dealing with InSAR techniques and products, at least in terms of technology limits, noise sources and accuracy analyses, thus leading to properly identify possible anomalies and correctly interpret the InSAR-derived results.

Unfortunately, the broad development of advanced InSAR techniques in the last decades has fostered their massive exploitation among a wide community of end-users coming from different scientific contexts, even not specifically experts in the InSAR field. Such a large variety of possible users dealing with InSAR deformation measurements associated with built-on structures has to be preliminarily qualified and, in some cases, guided by expert “eyes” throughout the interpretation of the InSAR-derived products. This is particularly demanded in the case of man-made structures

and infrastructures interested in failures or collapses that provoked casualties with serious legal implications, as for the case of the Morandi bridge, where the InSAR analyses should be carefully presented only after a deep and accurate assessment of the results and their interpretation.

In this study, we exploited the well established and extensively tested SBAS and TomoSAR MT-InSAR techniques to reprocess the same ascending and descending CSK datasets, relevant to the Morandi bridge, analyzed by Milillo et al. [2]. Our results show that, although we achieve denser coherent pixel maps relevant to the Morandi bridge, there is no evidence at all, even not for the results relevant to one of the processed orbits dataset or to the exploited SBAS and TomoSAR processing techniques, of the pre-collapse displacements reported in [2] in pixels located near the strands of the deck next to the collapsed pier. Accordingly, in our opinion, the pre-event InSAR study relevant to the Morandi bridge carried out by Milillo et al. [2] is an example of an InSAR deformation analysis affected by a false alarm.

Supplementary Materials: The following are available online at <http://www.mdpi.com/2072-4292/12/24/4011/s1>, Figure S1. Deformation mean velocity for the measurement points located at the ground level in correspondence to the area of interest of the collapsed pillar, (a) SBAS and (b) TomoSAR processing over the ascending dataset, (c) SBAS and (d) TomoSAR processing over the descending dataset; Figure S2. Plots of the estimated deformation time series for the measurement points at the ground level in correspondence to the area of interest of the collapsed pillar provided in Figure S1 for (a) SBAS and (b) TomoSAR processing over the ascending dataset, (c) SBAS and (d) TomoSAR processing over the descending dataset.

Author Contributions: R.L. conceived and supervised the overall work and contributed to the paper; D.R., M.B. and S.V. performed the processing of the CSK datasets, analyzed the achieved results and contributed to the paper; Y.M. contributed to the SBAS processing chain; G.F. and D.R. coordinated the TomoSAR processing; M.B. and F.C. supervised the SBAS processing; M.M. coordinated and supervised the SBAS implementation and processing. All authors have read and agreed to the published version of the manuscript.

Funding: This work was supported by the Italian Civil Protection Department, the ESA's GEP project, the EPOS-IP project of the European Union Horizon 2020 research and innovation program (grant agreement 676564), and the I-AMICA (PONa3_00363) project.

Acknowledgments: The contents of this Comment represent the Authors' ideas and do not necessarily correspond to the official opinion and policies of the Italian Civil Protection Department. The Authors wish to thank Simone Guarino, Ferdinando Parisi and Maria Consiglia Rasulo of the Institute for the Electromagnetic Sensing of the Environment, Italian National Research Council, for their continuous technical assistance. CSK SAR data are acquired through the Italian Space Agency and Italian Civil Protection Department agreement; the Digital Elevation Models of the analyzed area are acquired through the NASA SRTM archive.

Conflicts of Interest: The authors declare no conflict of interest.

References

1. Genova, le 43 Vittime del Crollo del Ponte Morandi. Available online: https://www.ansa.it/liguria/notizie/2018/08/18/-le-43-vittime-del-crollo-del-ponte-morandi_9f53cd46-1b85-45ae-a23a-dc92c9c5cef3.html (accessed on 3 December 2020).
2. Milillo, P.; Giardino, G.; Perissin, D.; Milillo, G.; Coletta, A.; Terranova, C. Pre-Collapse Space Geodetic Observations of Critical Infrastructure: The Morandi Bridge, Genoa, Italy. *Remote Sens.* **2019**, *11*, 1403. [CrossRef]
3. Bonano, M.; Manunta, M.; Pepe, A.; Paglia, L.; Lanari, R. From previous C-band to new X-band SAR systems: Assessment of the DInSAR mapping improvement for deformation time-series retrieval in urban areas. *IEEE Trans. Geosci. Remote Sens.* **2013**, *51*, 1973–1984. [CrossRef]
4. Sansosti, E.; Berardino, P.; Bonano, M.; Calò, F.; Castaldo, R.; Casu, F.; Manunta, M.; Manzo, M.; Pepe, A.; Pepe, S.; et al. How second generation SAR systems are impacting the analysis of ground deformation. *Int. J. Appl. Earth Obs. Geoinf.* **2014**, *28*, 1–11. [CrossRef]
5. Berardino, P.; Fornaro, G.; Lanari, R.; Sansosti, E. A New Algorithm for Surface Deformation Monitoring Based on Small Baseline Differential SAR Interferograms. *IEEE Trans. Geosci. Remote Sens.* **2002**, *40*, 2375–2383. [CrossRef]
6. Lanari, R.; Mora, O.; Manunta, M.; Mallorquí, J.J.; Berardino, P.; Sansosti, E. A small-baseline approach for investigating deformations on full-resolution differential SAR interferograms. *IEEE Trans. Geosci. Remote Sens.* **2004**, *42*, 1377–1386. [CrossRef]

7. Bonano, M.; Manunta, M.; Marsella, M.; Lanari, R. Long-term ERS/ENVISAT deformation time-series generation at full spatial resolution via the extended SBAS technique. *Int. J. Remote Sens.* **2012**, *33*, 4756–4783. [[CrossRef](#)]
8. Fornaro, G.; Reale, D.; Serafino, F. Four-Dimensional SAR Imaging for Height Estimation and Monitoring of Single and Double Scatterers. *IEEE Trans. Geosci. Remote Sens.* **2009**, *47*, 224–237. [[CrossRef](#)]
9. Fornaro, G.; Lombardini, F.; Pauciuolo, A.; Reale, D.; Viviani, F. Tomographic Processing of Interferometric SAR Data: Developments, applications, and future research perspectives. *IEEE Signal Process. Mag.* **2014**, *31*, 41–50. [[CrossRef](#)]
10. Manunta, M.; Marsella, M.; Zeni, G.; Sciotti, M.; Atzori, S.; Lanari, R. Two-scale surface deformation analysis using the SBAS-DInSAR technique: A case study of the city of Rome, Italy. *Int. J. Remote Sens.* **2008**, *29*, 1665–1684. [[CrossRef](#)]
11. Arangio, S.; Calò, F.; Di Mauro, M.; Bonano, M.; Marsella, M.; Manunta, M. An application of the SBAS-DInSAR technique for the assessment of structural damage in the city of Rome. *Struct. Infrastruct. Eng.* **2014**, *10*, 1469–1483. [[CrossRef](#)]
12. Fornaro, G.; Verde, S.; Reale, D.; Pauciuolo, A. CAESAR: An Approach Based on Covariance Matrix Decomposition to Improve Multibaseline-Multitemporal Interferometric SAR Processing. *IEEE Trans. Geosci. Remote Sens.* **2015**, *53*, 2050–2065. [[CrossRef](#)]
13. Scifoni, S.; Bonano, M.; Marsella, M.; Sonnessa, A.; Tagliafierro, V.; Manunta, M.; Lanari, R.; Ojha, C.; Sciotti, M. On the joint exploitation of long-term DInSAR time series and geological information for the investigation of ground settlements in the town of Roma (Italy). *Remote Sens. Environ.* **2016**, *182*, 113–127. [[CrossRef](#)]
14. Solari, L.; Ciampalini, A.; Raspini, F.; Bianchini, S.; Zinno, I.; Bonano, M.; Manunta, M.; Moretti, S.; Casagli, N. Combined use of C- and X-band SAR data for subsidence monitoring in an urban area. *Geosciences* **2017**, *7*, 21. [[CrossRef](#)]
15. Wang, Y.; Zhu, X.X.; Shi, Y.; Bamler, R. Operational TomoSAR processing using TerraSAR-X high resolution spotlight stacks from multiple view angles. In Proceedings of the 2012 IEEE International Geoscience and Remote Sensing Symposium, Munich, Germany, 22–27 July 2012; pp. 7047–7050. [[CrossRef](#)]
16. Zhu, M.; Wan, X.; Fei, B.; Qiao, Z.; Ge, C.; Minati, F.; Vecchioli, F.; Li, J.; Costantini, M. Detection of Building and Infrastructure Instabilities by Automatic Spatiotemporal Analysis of Satellite SAR Interferometry Measurements. *Remote Sens.* **2018**, *10*, 1816. [[CrossRef](#)]
17. Zhu, X.X. Very High Resolution Tomographic SAR Inversion for Urban Infrastructure Monitoring—A Sparse and Nonlinear Tour. Ph.D. Thesis, Technische Universität München, Verlag der Bayerischen Akademie der Wissenschaften, München, Germany, 2011.
18. Reale, D.; Fornaro, G.; Pauciuolo, A.; Zhu, X.; Bamler, R. Tomographic Imaging and Monitoring of Buildings with Very High Resolution SAR Data. *IEEE Geosci. Remote Sens. Lett.* **2011**, *8*, 661–665. [[CrossRef](#)]
19. Fornaro, G.; Reale, D.; Verde, S. Bridge thermal dilation monitoring with millimeter sensitivity via multidimensional SAR imaging. *IEEE Geosci. Remote Sens. Lett.* **2013**, *10*, 677–681. [[CrossRef](#)]
20. Reale, D.; Noviello, C.; Verde, S.; Cascini, L.; Terracciano, G.; Arena, L. A multi-disciplinary approach for the damage analysis of cultural heritage: The case study of the St. Gerlando Cathedral in Agrigento. *Remote Sens. Environ.* **2019**, *235*, 111464. [[CrossRef](#)]
21. Franceschetti, G.; Lanari, R. *Synthetic Aperture Radar Processing*; CRC Press: Boca Raton, FL, USA, 1999.
22. Grandoni, D.; Battagliere, M.L.; Daraio, M.G.; Sacco, P.; Coletta, A.; Di Federico, A.; Mastracci, F. Space-based technology for emergency management: The COSMO-SkyMed constellation contribution|Copernicus Emergency Management Service. *Procedia Technol.* **2014**, *16*, 858–866. [[CrossRef](#)]
23. Zebker, H.A.; Villasenor, J. Decorrelation in interferometric radar echoes. *IEEE Trans. Geosci. Remote Sens.* **1992**, *30*, 950–959. [[CrossRef](#)]
24. Casu, F.; Manzo, M.; Lanari, R. A quantitative assessment of the SBAS algorithm performance for surface deformation retrieval from DInSAR data. *Remote Sens. Environ.* **2006**, *102*, 195–210. [[CrossRef](#)]
25. Pepe, A.; Sansosti, E.; Berardino, P.; Lanari, R. On the generation of ERS/ENVISAT DInSAR time-series via the SBAS technique. *IEEE Geosci. Remote Sens. Lett.* **2005**, *2*, 265–269. [[CrossRef](#)]
26. Notti, D.; Calò, F.; Cigna, F.; Manunta, M.; Herrera, G.; Berti, M.; Meisina, C.; Tapete, D.; Zucca, F. A User-Oriented Methodology for DInSAR Time Series Analysis and Interpretation: Landslides and Subsidence Case Studies. *Pure Appl. Geophys.* **2015**, *172*, 3081–3105. [[CrossRef](#)]

27. D’Auria, L.; Pepe, S.; Castaldo, R.; Giudicepietro, F.; Macedonio, G.; Ricciolino, P.; Tizzani, P.; Casu, F.; Lanari, R.; Manzo, M.; et al. Magma injection beneath the urban area of Naples: A new mechanism for the 2012–2013 volcanic unrest at Campi Flegrei caldera. *Sci. Rep.* **2015**, *5*, 13100. [[CrossRef](#)] [[PubMed](#)]
28. Fernández, J.; Tizzani, P.; Manzo, M.; Borgia, A.; González, P.J.; Martí, J.; Pepe, A.; Camacho, A.G.; Casu, F.; Berardino, P.; et al. Gravity-driven deformation of Tenerife measured by InSAR time series analysis. *Geophys. Res. Lett.* **2009**, *36*, L04306. [[CrossRef](#)]
29. Lanari, R.; Berardino, P.; Bonano, M.; Casu, F.; Manconi, A.; Manunta, M.; Manzo, M.; Pepe, A.; Pepe, S.; Sansosti, E.; et al. Surface displacements associated with the L’Aquila 2009 Mw 6.3 earthquake (central Italy): New evidence from SBAS-DInSAR time series analysis. *Geophys. Res. Lett.* **2010**, *37*, L20309. [[CrossRef](#)]
30. Diao, F.; Walter, T.R.; Solaro, G.; Wang, R.; Bonano, M.; Manzo, M.; Ergintav, S.; Zheng, Y.; Xiong, X.; Lanari, R. Fault locking near Istanbul: Indication of earthquake potential from InSAR and GPS observations. *Geophys. J. Int.* **2016**, *205*, 490–498. [[CrossRef](#)]
31. Calò, F.; Ardizzone, F.; Castaldo, R.; Lollino, P.; Tizzani, P.; Guzzetti, F.; Lanari, R.; Angeli, M.G.; Pontoni, F.; Manunta, M. Enhanced landslide investigations through advanced DInSAR techniques: The Ivancich case study, Assisi, Italy. *Remote Sens. Environ.* **2014**, *142*, 69–82. [[CrossRef](#)]
32. Cignetti, M.; Manconi, A.; Manunta, M.; Giordan, D.; De Luca, C.; Allasia, P.; Ardizzone, F. Taking Advantage of the ESA G-POD Service to Study Ground Deformation Processes in High Mountain Areas: A Valle d’Aosta Case Study, Northern Italy. *Remote Sens.* **2016**, *8*, 852. [[CrossRef](#)]
33. Zhao, Q.; Pepe, A.; Gao, W.; Lu, Z.; Bonano, M.; He, M.L.; Wang, J.; Tang, X. A DInSAR investigation of the ground settlement time evolution of ocean-reclaimed lands in Shanghai. *IEEE J. Sel. Top. Appl. Earth Obs. Remote Sens.* **2015**, *8*, 1763–1781. [[CrossRef](#)]
34. Zeni, G.; Bonano, M.; Casu, F.; Manunta, M.; Manzo, M.; Marsella, M.; Pepe, A.; Lanari, R. Long-term deformation analysis of historical buildings through the advanced SBAS-DInSAR technique: The case study of the city of Rome, Italy. *J. Geophys. Eng.* **2011**. [[CrossRef](#)]
35. Ferretti, A.; Prati, C.; Rocca, F. Permanent Scatterers in SAR Interferometry. *IEEE Trans. Geosci. Remote Sens.* **2001**, *39*, 8–20. [[CrossRef](#)]
36. Ferretti, A.; Fumagalli, A.; Novali, C.; Prati, C.; Rocca, F.; Rucci, A. A new algorithm for processing interferometric data-stacks: SqueeSAR. *IEEE Trans. Geosci. Remote Sens.* **2011**, *49*, 3460–3470. [[CrossRef](#)]
37. Fornaro, G.; Serafino, F.; Soldovieri, F. Three-dimensional focusing with multipass SAR data. *IEEE Trans. Geosci. Remote Sens.* **2003**, *41*, 507–517. [[CrossRef](#)]
38. Gini, F.; Lombardini, F.; Montanari, M. Layover solution in multibaseline SAR Interferometry. *IEEE Trans. Aerosp. Electron. Syst.* **2002**, *38*, 1344–1356. [[CrossRef](#)]
39. Reigber, A.; Moreira, A. First demonstration of airborne SAR tomography using multibaseline L-band data. *IEEE Trans. Geosci. Remote Sens.* **2000**, *38*, 2142–2152. [[CrossRef](#)]
40. Lombardini, F. Differential Tomography: A new framework for SAR Interferometry. *IEEE Trans. Geosci. Remote Sens.* **2005**, *43*, 37–44. [[CrossRef](#)]
41. Reale, D.; Fornaro, G.; Pauciuolo, A. Extension of 4-D SAR Imaging to the Monitoring of Thermally Dilating Scatterers. *IEEE Trans. Geosci. Remote Sens.* **2013**, *51*, 5296–5306. [[CrossRef](#)]
42. Zhu, X.X.; Bamler, R. Let’s Do the Time Warp: Multicomponent Nonlinear Motion Estimation in Differential SAR Tomography. *IEEE Geosci. Remote Sens. Lett.* **2011**, *8*, 735–739. [[CrossRef](#)]
43. Fornaro, G.; Pauciuolo, A.; Serafino, F. Deformation monitoring over large areas with multipass differential SAR interferometry: A new approach based on the use of spatial differences. *Int. J. Remote Sens.* **2009**. [[CrossRef](#)]
44. De Maio, A.; Fornaro, G.; Pauciuolo, A. Detection of Single Scatterers in Multidimensional SAR Imaging. *IEEE Trans. Geosci. Remote Sens.* **2009**, *47*, 2284–2297. [[CrossRef](#)]
45. Ministero delle Infrastrutture e dei Trasporti, Consiglio Superiore dei Lavori Pubblici. Linee Guida per la Classificazione e Gestione del Rischio, la Valutazione della Sicurezza ed il Monitoraggio dei Ponti Esistenti. Available online: https://www.mit.gov.it/sites/default/files/media/notizia/2020-05/1_Testo_Linee_Guida_ponti.pdf (accessed on 3 December 2020).

Publisher’s Note: MDPI stays neutral with regard to jurisdictional claims in published maps and institutional affiliations.



© 2020 by the authors. Licensee MDPI, Basel, Switzerland. This article is an open access article distributed under the terms and conditions of the Creative Commons Attribution (CC BY) license (<http://creativecommons.org/licenses/by/4.0/>).